

The Origin of Supermassive Black Holes from Pop III.1 Seeds

Jonathan C. Tan

*Dept. of Space, Earth & Environment, Chalmers Univ. of Technology, Gothenburg, Sweden,
and Dept. of Astronomy, University of Virginia, Charlottesville, VA, USA
jctan.astro@gmail.com*

Jasbir Singh

INAF - Astronomical Observatory of Brera, via Brera 28, I-20121 Milan, Italy

Vieri Cammelli

*University of Trieste & INAF - AOT, via G.B. Tiepolo 11, I-34143 Trieste, Italy
and Dept. of Space, Earth & Environment, Chalmers Univ. of Technology*

Mahsa Sanati

*University of Oxford, Keble Road, Oxford OX1 3RH, UK
and Dept. of Space, Earth & Environment, Chalmers Univ. of Technology*

Maya Petkova

Dept. of Space, Earth & Environment, Chalmers Univ. of Technology, Gothenburg, Sweden

Devesh Nandal

Dept. of Astronomy, University of Virginia, Charlottesville, VA, USA

Pierluigi Monaco

University of Trieste & INAF - AOT, via G.B. Tiepolo 11, I-34143 Trieste, Italy

The origin of supermassive black holes (SMBHs) is a key open question for contemporary astrophysics and cosmology. Here we review the features of a cosmological model of SMBH formation from Pop III.1 seeds, i.e., remnants of metal-free stars forming in locally-isolated minihalos, where energy injection from dark matter particle annihilation alters the structure of the protostar allowing growth to supermassive scales (Banik et al. 2019; Singh et al. 2023; Cammelli et al. 2024). The Pop III.1 model explains the paucity of intermediate-mass black holes (IMBHs) via a characteristic SMBH seed mass of $\sim 10^5 M_{\odot}$ that is set by the baryonic content of minihalos. Ionization feedback from supermassive Pop III.1 stars sets the cosmic number density of SMBHs to be $n_{\text{SMBH}} \lesssim 0.2 \text{ Mpc}^{-3}$. The model then predicts that all SMBHs form by $z \sim 20$ with a spatial distribution that is initially unclustered. SMBHs at high redshifts $z \gtrsim 7$ should all be single objects, with SMBH binaries and higher order multiples emerging only at lower redshifts. We also discuss the implications of this model for SMBH host galaxy properties, occupation fractions, gravitational wave emission, cosmic reionization, and the nature of dark matter. These predictions are compared to latest observational results, especially from HST, JWST and pulsar timing array observations.

1. Introduction

The origin of supermassive black holes (SMBHs) that manifest themselves as active galactic nuclei (AGN) in the centers of most large galaxies is one of the most pressing open questions of current astrophysics and cosmology. How do these cosmic behemoths come into being? The discovery of SMBHs as $z \sim 7 - 10$ AGN (e.g., Wang et al. 2021, Bogdán et al. 2024; Maiolino et al. 2024a; Fig. 1) indicates that at least some SMBHs formed very early, during the so-called “dark ages” of the Universe, and did so with initial “seed” masses already in the supermassive regime, i.e., $\sim 10^5 M_\odot$. While sustained growth at super-Eddington rates could allow lower-mass seeds, there is little evidence for such accretion rates in observed samples of lower-redshift quasars (e.g., Wu & Shen 2022; Zeltyn et al. 2024), while the handful of examples of high- z luminous quasars with Eddington ratios of up to ~ 2 (Yang et al. 2021) are consistent with obeying the Eddington limit given measurement uncertainties. Furthermore, the apparent dearth of intermediate-mass black holes (IMBHs) (e.g., Reines & Comastri 2016; Baumgart 2017; Greene et al. 2020; Mummery & van Velzen 2024) suggests that a mass scale of $\sim 10^5 M_\odot$ is a characteristic feature of SMBH formation and that this is widely separated from the $\sim 10 - 100 M_\odot$ black holes that are the remnants of standard stellar populations.

A wide variety of SMBH formation theories have been proposed (see reviews by, e.g., Rees 1978; Volonteri et al. 2021). Most, including formation in dense stellar clusters (e.g., Gürkan et al. 2004; Freitag et al. 2006; Schleicher et al. 2022) or the popular “Direct Collapse” from massive ($\sim 10^8 M_\odot$), atomically-cooled, metal-free, irradiated and/or turbulent halos (e.g., Haehnelt & Rees 1993; Bromm & Loeb 2003; Chon et al. 2016; Wise et al. 2019; Latif et al. 2022), struggle to explain a characteristic mass scale of SMBHs of $\sim 10^5 M_\odot$, i.e., formation of IMBHs would be expected to be much more common in these scenarios. Furthermore, these models have great difficulty in seeding *all* SMBHs, i.e., to yield the numbers seen in the local Universe, i.e., $n_{\text{SMBH}} \gtrsim 5 \times 10^{-3} \text{Mpc}^{-3}$ (Vika et al. 2009; BTM19). In the context of direct collapse black holes (DCBHs), Chon et al. (2016) performed hydrodynamic (HD) simulations of a $(\sim 30 \text{Mpc})^3$ volume and estimated a co-moving number density of SMBH seeds to be only $n_{\text{SMBH}} \sim 10^{-4} \text{Mpc}^{-3}$. Wise et al. (2019) carried out radiation-HD simulations and estimated a global co-moving number density of DCBHs to be much smaller, i.e., at a level of $\sim 10^{-7} - 10^{-6} \text{Mpc}^{-3}$. The study of Latif et al. (2022) of turbulence-supported halos also yields similar constraints of $n_{\text{SMBH}} < 10^{-6} \text{Mpc}^{-3}$. For formation from dense star clusters, it is difficult to calculate the occurrence rate of the conditions for efficient runaway growth. However the densities needed in the models of Gürkan et al. (2004) and Freitag et al. (2006) are almost never seen in local populations of young clusters (e.g., Tan et al. 2014).

One theory that aims to address the above features of the SMBH population and form it with a single mechanism is SMBH birth from Population III.1 stars (Banik, Tan & Monaco 2019 [BTM19]; Singh, Monaco & Tan 2023 [SMT23]; Cammelli et al. 2024 [CMT24]). Here we review the key features of the Pop III.1 model.

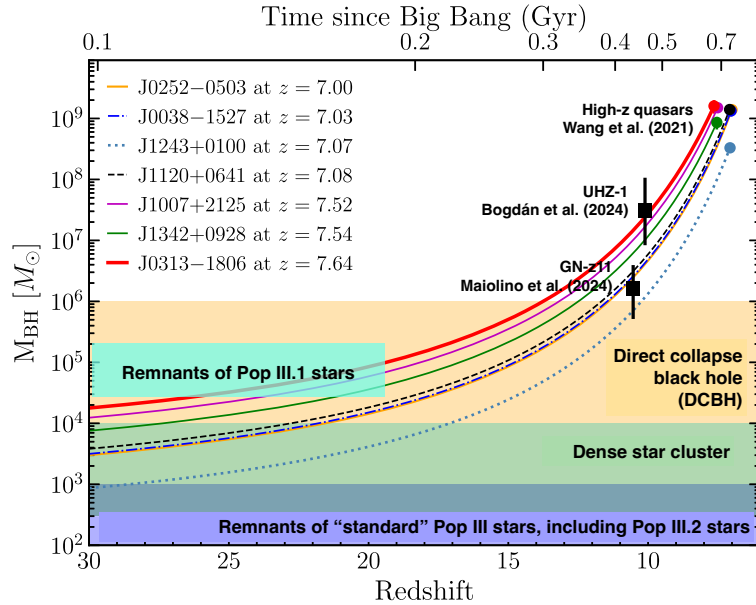


Fig. 1. (adapted from Wang et al. 2021) Black hole growth tracks of a sample of $z > 7$ quasars (circles) with the assumption of continuous Eddington-limited accretion, i.e., with quasar luminosity $L = \epsilon mc^2 = L_{\text{Edd}}$ and a radiative efficiency of $\epsilon = 0.1$. The curves give the mass of seed black holes required to grow to the observed mass of each SMBH in these quasars. With the above assumptions, these SMBHs require supermassive ($\sim 10^5 M_{\odot}$) seeds if the formation redshifts are $\sim 15 - 20$. The AGN at $z = 10.1$ (UHZ-1, Bogdan et al. 2024) and $z = 10.6$ (GN-z11, Maiolino et al. 2024) are also shown (black squares), with similar implications. Shaded regions show mass scales of “standard” Pop III stellar remnants (purple), IMBHs that may form in dense stellar clusters (green), direct collapse black holes (yellow), and Pop III.1 remnants (light blue) (see text).

2. Pop III.1 Protostars - Impact of Dark Matter Annihilation

Pop III.1 protostars are the first dense structures to form in their local region of the Universe, situated at the center of “isolated” (i.e., undisturbed by radiative or chemical feedback from other astrophysical sources) dark matter minihalos, i.e., with total masses of $\sim 10^6 M_{\odot}$. Under these conditions collapse of metal-free gas to high densities occurs co-located with the peak of dark matter density. Previous work on “standard” Pop III star formation in such minihalos reached a near consensus view that the masses of the stars formed are $\sim 100 - 10^3 M_{\odot}$ set by internal ionizing feedback (e.g., Abel et al. 2002; Bromm et al. 2002; Tan & McKee 2004; McKee & Tan 2008; Tan et al. 2010; Hosokawa et al. 2011; Hirano et al. 2014; Susa et al. 2014; Tanaka et al. 2017). Such stars would produce, at best, “light” seeds, i.e., $\lesssim 10^3 M_{\odot}$ that would have difficulties in explaining the observed high- z AGN.

However, as first pointed out by Spolyar, Freese & Gondolo (2008), weakly interacting massive particle (WIMP) dark matter annihilation (DMA) heating could have a major impact on Pop III star formation. In models in which the WIMP is

4 *J. C. Tan et al.*

its own anti-particle and self-annihilates with a rate coefficient given by $\langle\sigma_a v\rangle \simeq 3 \times 10^{-26} \text{ cm}^3 \text{ s}^{-1}$ (e.g., Jungman et al. 1996), i.e., to explain the cosmic dark matter density, $\Omega_{\text{DM}} = 0.268$, then a large fraction, $\sim 2/3$, of the energy, i.e., the non-neutrino component consisting of high energy photons and electron-positron pairs, is expected to be trapped in the star. The rate of energy injection is boosted by many orders of magnitude if the local dark matter density is enhanced by adiabatic contraction during slow, monolithic contraction of the H/He gas in the minihalo.

Natarajan, Tan & O’Shea (2009) examined several example simulated minihalos confirming the results of Spolyar et al. (2008) that DMA heating would become important in Pop III.1 protostars, including setting their initial structures. Smith et al. (2012) and Stacey et al. (2014) carried out simulations of the first stages of Pop III.1 star formation including the effects of WIMP annihilation on the chemistry and thermodynamics of the collapse. These simulations found that by including WIMP DMA heating there was much reduced fragmentation during the collapse, supporting the likelihood that single massive star formation results from each Pop III.1 minihalo. In addition, the amplification of magnetic fields in Pop III accretion disks (Tan & Blackman 2004; Latif & Schleicher 2016) is also expected to inhibit fragmentation during the star formation process. However, the final outcome of Pop III.1 star formation from the simulations of Smith et al. and Stacey et al. remains uncertain, as they were only able to follow the growth of the star up to $\sim 10 M_{\odot}$.

Freese et al. (2010) and Rindler-Daller et al. (2015) presented models of protostellar evolution of DMA-powered protostars, which they refer to as “dark stars”, that continue to accrete to much higher masses. In the study of Rindler-Daller et al. (2015), starting with initial masses from 2 to $5 M_{\odot}$, the protostars were followed to $> 10^5 M_{\odot}$ for cases with WIMP masses of $m_{\chi} = 10, 100$ & 1000 GeV and gas accretion rates of 10^{-3} and $10^{-1} M_{\odot} \text{ yr}^{-1}$. Typical accretion rates in Pop III.1 minihalos are expected to be $\sim 10^{-2} M_{\odot} \text{ yr}^{-1}$ (Tan & McKee 2004), for which protostellar growth to $\sim 10^5 M_{\odot}$ would take $\sim 10^7 \text{ yr}$. The main feature of the protostellar evolution calculations of Rindler-Daller et al. is that the radius of the forming star remains very large (i.e., few $\times 10^3 R_{\odot}$) and the photospheric temperature relatively cool (i.e., $\sim 10^4 \text{ K}$). This implies that ionizing feedback from the protostar will be relatively weak compared to the case of standard Pop III star formation. However, in these models Pop III.1 protostellar temperatures start to rise above 10^4 K as m_* grows beyond $10^3 M_{\odot}$, so internal feedback processes do need to be considered. In particular, it remains to be demonstrated if the mass loss rate driven by internal photoevaporation of the disk remains small compared to the accretion rate. The photoevaporative mass loss rate is given by (McKee & Tan 2008):

$$\dot{m}_{\text{evap}} = 1.1 \times 10^{-4} S_{49} T_{3e4}^{0.4} m_{*d,3}^{1/2} M_{\odot} \text{ yr}^{-1}, \quad (1)$$

where $S_{49} \equiv S/10^{49} \text{ s}^{-1}$ is the protostellar H-ionizing (EUV) photon production rate, $T_{3e4} \equiv T/(3 \times 10^4 \text{ K})$ is the ionized gas temperature (with normalization appropriate for metal-free gas) and $m_{*d,3} \equiv m_{*d}/(10^3 M_{\odot})$ is the mass of the star-disk system.

Another limitation of the Rindler-Daller et al. (2015) models is that they do not

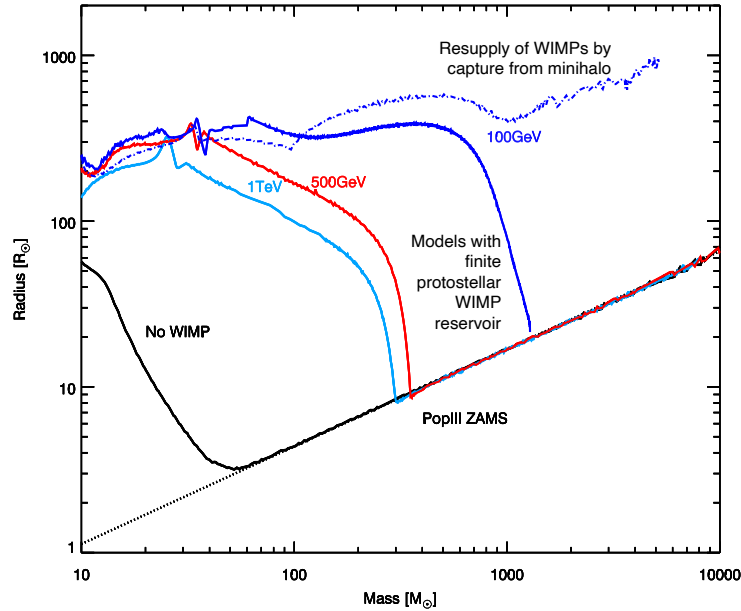


Fig. 2. MESA (Modules for Experiments in Stellar Astrophysics; Paxton et al. 2013) calculations of Pop III.1 protostars forming from a minihalo with accretion rate given by the isentropic accretion model of Tan & McKee (2004). The standard (“no WIMP”) case is shown by the black line, illustrating contraction to the zero age main sequence (ZAMS) structure by a mass of $\sim 50 M_{\odot}$. Accretion to higher masses along the ZAMS is expected to halt at $\sim 100 M_{\odot}$ because of photoevaporation feedback (e.g., McKee & Tan 2008; Tanaka et al. 2017). The light blue, red and dark blue solid lines show models in which the protostar inherits a fixed amount of WIMP dark matter based on its initial structure from the models of Natarajan et al. (2009). WIMP annihilation heating keeps the protostar in a swollen state until depletion of the initial WIMP reservoir by masses of ~ 300 to $1,000 M_{\odot}$. The dashed blue line shows a model that includes resupply of WIMPs by capture from the surrounding minihalo. Here, the evolution has been followed to $\sim 5,000 M_{\odot}$ with the star remaining in a large, swollen state up to this point. Note, the main effect of WIMP annihilation heating on protostellar structure is to keep the protostar large, cool, and with a low ionizing feedback, thus potentially allowing accretion to supermassive scales.

allow for depletion of WIMPs within the protostar: i.e., they make the assumption of “continuous replenishment” by capture of WIMPs from the surrounding minihalo. Figure 2 shows example Pop III.1 protostar calculations that relax this assumption. Several models with finite WIMP reservoirs, implied by the calculations of Natarajan et al. (2009) for various WIMP masses, are shown. In these cases, contraction to the ZAMS is delayed until the protostar has grown to at most $\sim 10^3 M_{\odot}$. At this point ionizing feedback would be expected to shut off growth of the star. However, a model in which the protostar is able to keep capturing WIMPs from the surrounding minihalo, also shown in Fig. 2, allows the protostar to remain large and relatively cool until at least $5,000 M_{\odot}$. Thus, as discussed by BTM19, it remains a plausible scenario that WIMP annihilation heating could keep the protostar large,

cool, and with relatively low ionizing feedback that allows efficient accretion of the baryonic content of the minihalo, i.e., $\sim 10^5 M_\odot$, to a central, supermassive star, which, after a brief lifetime, ultimately collapses to a SMBH of similar mass.

There are two main possibilities for how SMBH formation could occur in these Pop III.1 minihalos. The protostar may run out of WIMP support, i.e., fail to keep capturing enough WIMPs to maintain its luminosity, leading to eventual contraction to the zero age main sequence (ZAMS). At this point its ionizing feedback should shut off further accretion. It would then undergo main sequence and post main sequence stellar evolution, with the final outcome expected to be collapse of most of the stellar mass to a black hole (e.g., Heger & Woosley 2002). The other possibility is that the protostar keeps accreting. Then collapse to a SMBH may be induced by the star becoming unstable with respect to the general relativistic radial instability (GRRI). For non-rotating main-sequence stars, this is expected to occur at a mass of $\sim 5 \times 10^4 M_\odot$ (Chandrasekhar 1964), while in the case of maximal uniform rotation this is raised to $\sim 10^6 M_\odot$ (Baumgarte & Shapiro 1999).

There are a few cases of SMBHs with masses below $10^5 M_\odot$. For example, Häberle et al. (2024) have estimated the mass of the black hole in ω Cen, a stripped nucleus of a dwarf elliptical galaxy, to be in the range $0.8 - 5 \times 10^4 M_\odot$. Another example is the dwarf galaxy RGG 118, which is estimated to host a $\sim 5 \times 10^4 M_\odot$ nuclear BH (Baldassare et al. 2015). The results of Mummery & van Velzen (2024) imply the existence of a small number of SMBHs just below $\sim 10^5 M_\odot$. Pop III.1 protostars are likely to have some rotational support and thus would not reach the GRRI limit until $> 10^5 M_\odot$. Thus, we consider that the most likely scenario involves Pop III.1 protostars running out of WIMP support at mass scales $\gtrsim 10^4 M_\odot$ and undergoing a phase of main sequence and post main sequence nuclear burning before a core collapse supernova explosion leads to efficient SMBH formation.

3. Pop III.1, Pop III.2 and Cosmic Number Density of SMBHs

The main parameter of the Pop III.1 theory is the “isolation distance”, d_{iso} , that Pop III.1 halos need to be separated from other astrophysical sources of radiation (see Fig. 3). If a minihalo is too close to a source of EUV radiation, i.e., closer than d_{iso} , then its free electron abundance is enhanced leading to greater rates of H_2 formation, enhanced cooling rates and higher degrees of fragmentation to lower-mass ($\sim 10 M_\odot$) Pop III.2 stars (Greif & Bromm 2006; Johnson & Bromm 2006). Fragmentation would imply that slow, monolithic contraction of gas in the minihalo does not occur so that dark matter densities are not enhanced via adiabatic contraction so that there is a negligible impact of DMA heating on protostellar evolution. Thus Pop III.2 minihalos do not give rise to SMBH seeds.

One potential physical model for the isolation distance is the size of the ionized region around a supermassive Pop III.1 star. As discussed above, it is possible that such stars exist for several Myr in a phase on or near the main sequence, with photospheric temperatures of $\sim 10^5$ K. The peak of the spectral energy distribution

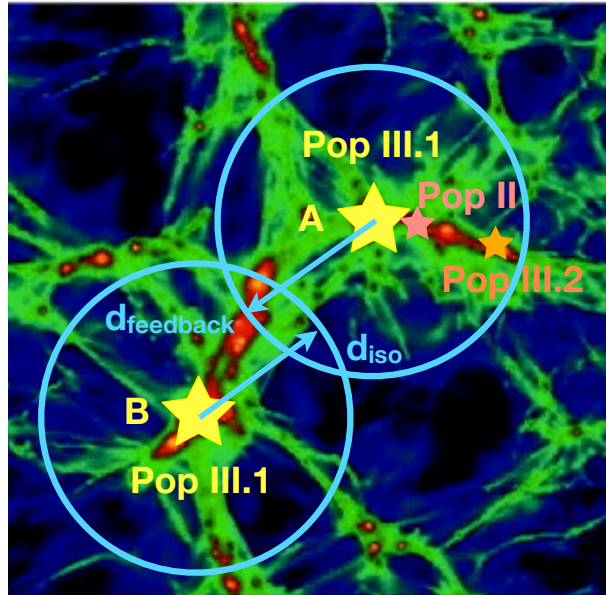


Fig. 3. Schematic diagram illustrating the definition of Pop III.1 minihalos, which are assumed to be SMBH progenitors, and Pop III.2 minihalos, which form stars of $\sim 10 M_{\odot}$. Source A is the first to form in this local region of the Universe. It irradiates its surroundings out to a feedback distance, d_{feedback} , which prevents other Pop III.1 sources from forming. Instead, minihalos within this irradiated volume form Pop III.2 stars if they have not been polluted by stellar ejecta or Pop II stars if they have been. Source B forms next as another Pop III.1 source, i.e., being alone within an “isolation distance” d_{iso} , which is set equal to d_{feedback} .

of such a photosphere is at $\lambda_{\text{peak}} \simeq 0.029 \mu\text{m}$, corresponding to photon energies of $hc/\lambda = 43 \text{ eV}$. The luminosity of such a star is expected to be near that of the Eddington luminosity, i.e., $L_* \simeq L_{\text{Edd}} = 3.2 \times 10^9 (m_*/10^5 M_{\odot}) L_{\odot}$. Most of the photons emitted by the star have energies $> 13.6 \text{ eV}$ and so are able to ionize H and the rate of production of these photons is $S \simeq 10^{53} \text{ s}^{-1}$. Such a source would have an enormous impact on the surrounding intergalactic medium (IGM). The extent of the ionized region can be evaluated as the Strömgen radius:

$$R_S = \left(\frac{3}{4\pi} \frac{S}{\alpha^{(2)} n_e n_p} \right)^{1/3} = 61.3 S_{53}^{1/3} T_{3e4}^{0.27} \left(\frac{n_{\text{H}}}{n_{\text{H},z=30}} \right)^{-2/3} \text{ kpc}, \quad (2)$$

$$= 1.90 S_{53}^{1/3} T_{3e4}^{0.27} (n_{\text{H}}/n_{\text{H},z=30})^{-2/3} ([1 + z_{\text{form}}]/31) \text{ cMpc} \quad (3)$$

$$= 1.90 S_{53}^{1/3} T_{3e4}^{0.27} ([1 + z_{\text{form}}]/31)^{-1} \text{ cMpc} \quad (4)$$

where $\alpha^{(2)} = 1.08 \times 10^{-13} T_{3e4}^{-0.8} \text{ cm}^3 \text{ s}^{-1}$ is the recombination rate to excited states of ionized H, $S_{53} \equiv S/10^{53} \text{ s}^{-1}$, n_{H} is number density of H nuclei and $n_{\text{H},z=30} = 5.72 \times 10^{-3} \text{ cm}^{-3}$ is the average value of n_{H} in the IGM at a redshift of 30 (i.e.,

when most Pop III.1 sources are forming in the fiducial BTM19 scenario; see below). Note, for simplicity, we have ignored reionization of He.

However, the time to establish ionization equilibrium in these HII regions is relatively long, i.e., $t_{\text{ion}} \simeq (4/3)\pi R_S^3 n_{\text{H}}/S = (\alpha^{(2)} n_{\text{H}})^{-1} = 51.3[(1 + z_{\text{form}})/31]^{-3}$ Myr. This is much longer than the expected lifetime of a supermassive star, i.e., $\lesssim 3$ Myr, although residual DMA heating would prolong its life somewhat. Taking a fiducial lifetime of $t_* = 10$ Myr, we estimate the extent of an R-type expanding HII region:

$$R_R = \left(\frac{3t_* S}{4\pi n_{\text{H}}} \right)^{1/3} = 35.5 t_{*,10}^{1/3} S_{53}^{1/3} (n_{\text{H}}/n_{\text{H},z=30})^{-1/3} \text{ kpc} \quad (5)$$

$$= 1.10 t_{*,10}^{1/3} S_{53}^{1/3} (n_{\text{H}}/n_{\text{H},z=30})^{-1/3} (1 + z_{\text{form}})/31 \text{ cMpc} \quad (6)$$

$$= 1.10 t_{*,10}^{1/3} S_{53}^{1/3} \text{ cMpc}, \quad (7)$$

where $t_{*,10} = t_*/10$ Myr. Note, that the co-moving extent of an R-type HII region is independent of redshift. The above estimate for the radius of the HII region undergoing R-type expansion assumes fully ionized conditions inside R_R . To check this approximation, we evaluate the mean free path for ionizing photons as

$$\lambda_{\text{mfp}} = (n_{\text{H}} \sigma_{\text{p.i.}})^{-1} = 9.0 (n_{\text{H}}/n_{\text{H},z=30})^{-1} (h\nu/13.6 \text{ eV})^3 \text{ pc}. \quad (8)$$

Thus even for very energetic photons, i.e., with $h\nu \sim 100 \text{ keV}$, then λ_{mfp} approaches 3.6 kpc, which is still small compared to R_R .

Assuming feedback distance $d_{\text{feedback}} = R_R$ and that the isolation distance for Pop III.1 SMBH formation is set by this feedback, i.e., $d_{\text{iso}} = d_{\text{feedback}}$, we estimate a co-moving number density of SMBHs as

$$n_{\text{SMBH}} = \frac{3}{4\pi R_R^3} \rightarrow 0.18 t_{*,10}^{-1} S_{53}^{-1} \text{ cMpc}^{-3}. \quad (9)$$

This estimate can be viewed as an upper limit since it has assumed maximal close packing of the sources and ignored other contributions to the ionizing background from Pop III.2, Pop II and AGN sources.

One of the main predictions of the Pop III.1 model for SMBH formation is that all SMBHs form very early in the Universe and are born in locally isolated minihalos, i.e., as single SMBHs. Thus their initial distribution is relatively unclustered. Clustering and mergers of seeded halos would occur much later as large-scale structure develops. Another main prediction is the existence of large (~ 1 cMpc) HII regions around these first sources. These HII regions would have a large volume filling factor at high redshift, but would then recombine after a relatively short time, i.e., ~ 50 Myr. Nevertheless, the residual free electrons in these relic HII regions are reason for suppressing further SMBH formation, since they lead to enhanced H_2 formation in the affected Pop III.2 minihalos, resulting in fragmentation to $\sim 10 M_{\odot}$ stars. In the next section we review the results of implementation of the Pop III.1 seeding scheme in simulations of cosmological volumes.

The Origin of Supermassive Black Holes from Pop III.1 Seeds 9

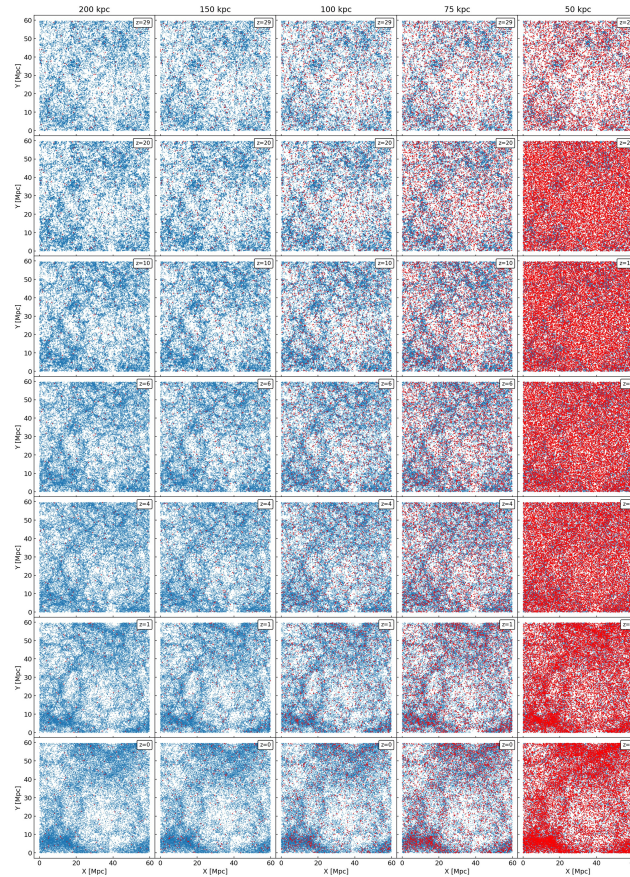


Fig. 4. (from SMT23) Projection of the positions of seeded haloes (red) and non-seeded haloes (blue) in the XY plane of a $(\sim 60 \text{ cMpc})^3$ volume for different isolation distances. The redshift is shown in the top right corner of each panel. Only the 30,000 most massive non-seeded haloes within each panel are shown for ease of visualization.

4. Cosmological Simulations of Pop III.1 Seeding of SMBHs and Comparison to Observational Constraints

BTM19 presented simulations of a $\sim (60 \text{ cMpc})^3$ volume using the PINOCCHIO (PINpointing Orbit Crossing Collapsed Hierarchical Objects) code (Monaco et al. 2002; Monaco et al. 2013), which uses a Lagrangian Perturbation Theory (LPT) based method (Moutarde et al. 1991; Buchert & Ehlers 1993; Catelan 1995) for the fast generation of catalogues of dark matter haloes in cosmological volumes. The BTM19 study had a dark matter particle mass resolution of $\sim 10^5 M_\odot$, so that minihaloes were resolved at a level of 10 particles per halo, sufficient to identify their location, and the evolution was followed down to $z = 10$. The isolation distance parameter, d_{iso} , was set equal to a constant value of proper distance, with values of

d_{iso} from 10 to 300 kpc explored. SMT23 extended this type of calculation down to $z = 0$. Figure 4 shows example outputs, i.e., projections of seeded and unseeded halos across the simulation volumes from high to low redshifts. SMT23 also explored an alternative seeding scheme based on a simple halo mass threshold (HMT), i.e., halos are seeded with a SMBH once they exceed a mass of $7.1 \times 10^{10} M_{\odot}$, which is a method commonly used in cosmological volume galaxy formation simulations, e.g., Illustris-TNG (Vogelsberger et al. 2014; Weinberger et al. 2017).

To better connect the predictions of the Pop III.1 SMBH seeding to observable galaxy properties one needs to implement a model of galaxy formation and evolution in the simulations. To this end, CMT24 applied the GALaxy Evolution and Assembly (GAEA) semi-analytic model (Fontanot et al. 2020) to the merger histories of the PINOCCHIO simulated halos. CMT24 considered Pop III.1 seeding for $d_{\text{iso}} = 50, 75$ and 100 kpc. They also compared these models with the HMT seeding model (with threshold halo mass of $7.1 \times 10^{10} M_{\odot}$) and with an All Light Seeds (ALS) seeding scheme, which seeds all halos with low-mass black holes.

4.1. *Co-Moving Number Density of SMBHs*

Figure 5 shows the redshift evolution of the co-moving number density of SMBHs, n_{SMBH} , for Pop III.1 models with d_{iso} from 50 to 200 kpc. Results of SMBH seeding based on an HMT above a mass of $7.1 \times 10^{10} M_{\odot}$ are also shown, as well as the Direct Collapse simulation of Chon et al. (2016). We see that the Pop III.1 models predict the existence of high number densities of SMBHs (and thus also AGN) at high z . A value of $d_{\text{iso}} = 100$ kpc is sufficient to produce $n_{\text{SMBH}} \simeq 5 \times 10^{-3} \text{ Mpc}^{-3}$, which is inferred from local SMBH populations (BTM19). However, it should be noted that, due to incompleteness, this is likely to be a lower limit. Thus smaller values of d_{iso} , i.e., closer to 50 kpc, may be needed. For values of $d_{\text{iso}} \gtrsim 50$ kpc, we see from Fig. 5 that essentially all SMBHs are in place by $z = 20$. After this n_{SMBH} remains nearly constant down to low redshifts, with only modest (up to $\sim 20\%$) decreases due to mergers that mainly occur at $z \lesssim 2$.

One of the main discoveries from early JWST observations has been the large numbers of AGN found at high redshifts. Fig. 5 shows estimates at $z = 4 - 7$ presented by Harikane et al. (2023), from the sample of Nakajima et al. (2023), with AGN identified by the presence of broad emission lines. These estimates, which involve an incompleteness correction down to a magnitude limit of $M_{\text{UV}} = -17$ mag, are lower bounds on n_{SMBH} , since fainter AGN are also expected to be present.

Hayes et al. (2024) carried out a re-observation of the Hubble Ultra Deep Field (HUDF) in 2023 using the Hubble Space Telescope (HST) with WFC3/IR in the F140W filter. This was designed to match the 2012 observation of Ellis et al. (2013) in the same filter in order to search for AGN via photometric variability. In addition, observations in 2009 (Bouwens et al. 2010) were compared with those of Ellis et al. in filters F105W and F160W. From a first examination of these data, three AGN were identified with high significance at $z = 6 - 7$. A variability

The Origin of Supermassive Black Holes from Pop III.1 Seeds 11

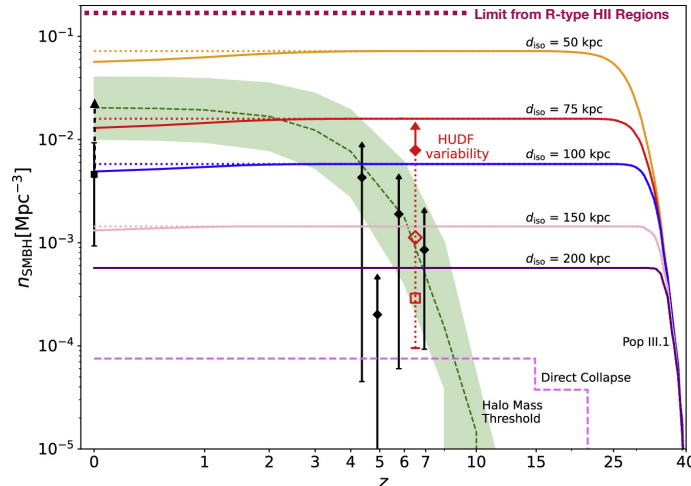


Fig. 5. Cosmic evolution of SMBH abundance. The comoving number density of SMBHs, n_{SMBH} , is plotted vs redshift, z . Various Pop III.1 formation models (BMT19; SMT23) with isolation distance parameters, d_{iso} , from 50 to 200 kpc (proper distance) are shown by the colored solid lines. At low redshifts, these decrease compared to the maximum value attained (dotted lines) due to mergers. The dark red dotted line at 0.18 Mpc^{-3} is the close-packed limiting value from the fiducial R-type HII region expansion model for d_{iso} (eq. 9). The green dashed line shows SMBH seeding based on an HMT above a mass of $7.1 \times 10^{10} M_{\odot}$ (Vogelsberger et al. 2014; Weinberger et al. 2017), with the shaded region illustrating a factor of 2 variation in this mass scale. The magenta dashed line shows results from a direct collapse model of SMBH formation (Chon et al. 2016). An observational constraint derived by counting $z = 6-7$ AGN in the HUDF variability survey (Hayes et al. 2024) is shown by the red open square, and the lower bound shows the Poisson uncertainty. The red open diamond corrects for variability incompleteness, and the red filled diamond is for luminosity incompleteness (corrected down to $M_{\text{UV}} = -17$ mag). Observational lower limits at $z = 0$ from local galaxies (BTM19) and at $z = 4-7$ from broad emission line AGN (Harikane et al. 2023) are shown with black square and diamonds, respectively.

incompleteness factor of ~ 5 is estimated (Cammelli et al., in prep.), given the recovery rate of 31 known AGN in the HUDF (Lyu et al. 2022). Luminosity incompleteness correction down to $M_{\text{UV}} = -17$ mag implies a factor of ~ 7 boost, yielding $n_{\text{SMBH}} \gtrsim 8 \times 10^{-2} \text{ cMpc}^{-3}$. From these results (and those of the more comprehensive analysis of the full dataset; Cammelli et al., in prep.) we infer $d_{\text{iso}} \lesssim 75 \text{ kpc}$. The measurements of n_{SMBH} at high z are strikingly similar to estimates in the local Universe and these begin to place meaningful constraints on both Pop III.1 and HMT type models.

4.2. Clustering of SMBHs

Since SMBHs are born isolated from other sources, i.e., by a distance d_{iso} , which is $\sim 1 - 3 \text{ cMpc}$, then SMBHs are predicted to have a low degree of initial spatial clustering. BTM19 and SMT23 found much lower levels of clustering of seeded halos, e.g., as measured via two-point angular or spatial correlation functions, com-

pared to equivalently massive halos selected independently of SMBH seeding. The level of SMBH clustering increased towards lower redshifts as large-scale structure developed, but the imprint of d_{iso} remained visible down to $z \sim 1$. Note, that the Pop III.1 model nevertheless predicts that SMBHs are found in highly biased regions, since these are the first-forming halos in each local region of the Universe. Comparisons of these results with the clustering properties of AGN (e.g., Hennawi et al. 2006; Hickox et al. 2009) will provide further tests of the Pop III.1 models.

4.3. Multiplicity of SMBHs

In the Pop III.1 scenario all SMBHs are born as single objects and, being isolated from each other, the level of binary and higher-order multiplicity, i.e., 2 or more SMBHs in the same halo, is very low at high z . Precise estimates of the binary SMBH fraction depend sensitively on the assumed timescales for galaxies to merge once halos have merged and for the lifetime of the SMBH pair within the same galaxy before their merger. However, from preliminary estimates (Singh 2024; Singh et al., in prep.) it is found that for $d_{\text{iso}} \gtrsim 75$ kpc there are essentially no binary AGN at $z > 5$. For $d_{\text{iso}} = 50$ kpc and an assumed halo to galaxy merger time of 500 Myr and a pair lifetime of 500 Myr, the binary SMBH fraction at $z \sim 5$ is $\sim 10^{-4}$, with the fraction rising to few $\times 10^{-2}$ by $z = 2$.

Yue et al. (2021) reported a close ($\lesssim 10$ kpc-scale) quasar pair at $z = 5.66$. They used this object to infer a lower limit on the SMBH pair fraction at $z = 5 - 6$ on scales < 30 kpc of $f_{\text{pair}} > 3 \times 10^{-3}$. Yue et al. (2023) reported discovery of a kpc-scale quasar pair at $z = 4.85$. Maiolino et al. (2024b) presented three high- z ($z = 4.1, 4.4, 5.9$) candidate dual AGN, but with multiplicity inferred only spectroscopically. Matsuoka et al. (2024) reported a quasar pair separated by 12 kpc in projected distance at $z = 6.05$. From these results, we infer that $d_{\text{iso}} \lesssim 50$ kpc is preferred. However, further work is needed to investigate the sensitivity of the Pop III.1 simulation results to assumed galaxy and SMBH merger timescales.

4.4. SMBHs and Galaxy Evolution

A main prediction of the Pop III.1 model is that SMBHs form before their eventual host galaxies. Thus the ratio of SMBH mass to host galaxy stellar mass will tend to be relatively large in high- z systems compared to those of the local Universe. However, detailed predictions of the co-evolution of SMBHs and galaxies are sensitive to the uncertain processes of star formation, SMBH fuelling, and feedback.

CMT24 have presented models of SMBH and galaxy co-evolution for the Pop III.1 seeding scenario based on the GAEA semi-analytic model (Fontanot et al. 2020). Figure 6 shows the evolution of the $M_{\text{BH}} - M_{\text{star}}$ relation of these models versus redshift, also comparing to an HMT model with threshold halo mass of $7.1 \times 10^{10} M_{\odot}$ for SMBH seeding and an All Light Seeds (ALS) model.

For the $M_{\text{BH}} - M_{\text{star}}$ relations at $z \sim 0$, compared to HMT and ALS, the Pop III.1 models tend to have: 1) larger dispersions; 2) shallower low-mass indices; 3)

The Origin of Supermassive Black Holes from Pop III.1 Seeds 13

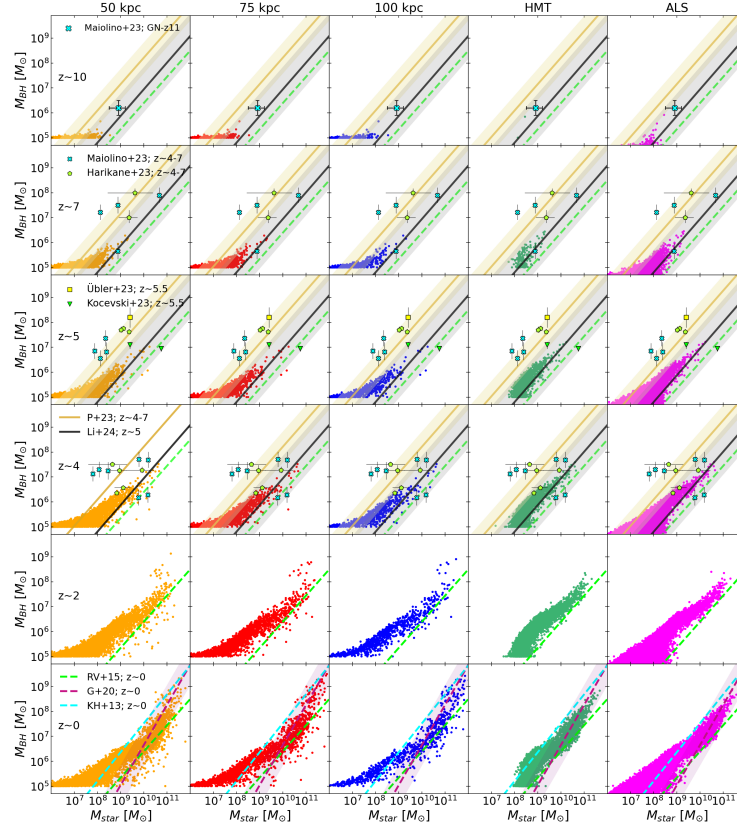


Fig. 6. (From CMT24) Scatter plot of the evolution of the $M_{\text{BH}} - M_{\text{star}}$ relation at several redshifts (rows, as labelled). First three columns are Pop III.1 seeding schemes with $d_{\text{iso}} = 50, 75, 100$ kpc. Fourth column is the fiducial Halo Mass Threshold (HMT) scheme and fifth column is the All Light Seed (ALS) scheme (see text). At redshift $z \sim 0$ several local empirical relations are shown: Kormendy & Ho (2013) (KH+13); Reines & Volonteri (2015) (RV+15); Greene et al. (2020) (G+20). At higher z the RV+15 $z = 0$ fit is shown for reference. High- z rows show comparison with JWST-detected AGN: in Pacucci et al. (2023), they directly fit the data in the redshift range $z \sim 4 - 7$, while Li et al. (2024) estimate an unbiased fit taking into account the uncertainties on the mass measurements and selection effects. Shaded regions illustrate the intrinsic scatter at $1-\sigma$ according to each relation. Colored symbols show faint AGN from Maiolino et al. (2024b); Harikane et al. (2023); Übler et al. (2023); Kocevski et al. (2023) and reported according to their redshifts. In the top row, results at $z \sim 10$ are shown against the single data point (GN-z11) from Maiolino et al. (2024).

steeper high-mass indices; 4) a larger number of the most massive SMBHs. As discussed by CMT24, these differences are potentially testable via comparison with censuses of local SMBH populations, including via comparison to SMBH mass functions (e.g., Mutlu-Pakdil et al. 2016; Shankar et al. 2020; Liepold & Ma 2024).

At redshifts of $z \sim 5$, the differences between the different seeding models for

the $M_{\text{BH}} - M_{\text{star}}$ relation are relatively modest. The overall normalization and index of these relations are consistent with the high- z estimate of Li et al. (2024), which, because of different analysis methods affecting accounting for survey biases, is about 1 dex below the relation inferred by Pacucci et al. (2023) from similar data.

Only at the highest redshifts, $z \gtrsim 7$ do differences between seeding schemes become more pronounced. For HMT this is because of the lack of massive halos and thus SMBHs at these redshifts. For ALS the black holes and galaxies grow together from very low masses, but by $z \sim 10$ there can be examples of $\sim 10^6 M_{\odot}$ SMBHs that are comparable to GN-z11. All models struggle to reach the $\sim 10^7 - 10^8 M_{\odot}$ masses of the JWST samples. This may be caused by the simulated box being quite small, i.e., $\sim (60 \text{ Mpc})^3$, and the observed AGN being quite rare objects. Or it may reflect limitations in the semi-analytic SMBH growth model.

To investigate this issue further, using the RAMSES code (Rosdahl et al. 2013), full radiation hydro simulations of SMBH growth and galaxy formation around a Pop III.1 seed have been implemented (Sanati et al., in prep.). A supermassive star phase with $S_{53} = 1$ for 10 Myr is implemented in the first minihalo of a $(7 \text{ Mpc})^3$ volume. We note that while this minihalo is identified at $z = 29$, it takes ~ 50 Myr, i.e., $z \sim 22$, for gas to reach high enough densities for Pop III.1 star formation. Following the assumed 10 Myr lifetime, when surrounding gas is mostly ionized, the source is then converted into a sink particle of mass $10^5 M_{\odot}$ that represents the growing SMBH, including its thermal, kinetic and radiative feedback. By $z = 9$ the SMBH has reached $\sim 3 \times 10^7 M_{\odot}$, while the host galaxy has $M_{\text{star}} \sim 10^8 M_{\odot}$. Such properties are similar to the JWST-detected systems at $z \gtrsim 7$.

Predictions for the luminosity functions of high- z AGN and galaxies of CMT24 have been carried out (Cammelli et al., in prep.). The overall luminosity function, i.e., of both seeded and unseeded galaxies, matches observed data well in the range $M_{\text{UV}} \gtrsim -22$ mag out to $z \sim 10$. A main feature of the Pop III.1 models is the relatively high and constant amplitude of the AGN + host galaxy luminosity function at $z \gtrsim 7$, especially in comparison to that of the HMT model. We note that larger volumes are needed to sample rare objects (relevant to $M_{\text{UV}} \lesssim -22$ mag).

Finally, as discussed by Ilie et al. (2023), we note that emission from Pop III.1 supermassive stars themselves may contribute to the observed luminosity functions, especially at the highest redshifts. Ilie et al. have modeled JWST-detected sources out to $z \simeq 14$ with supermassive ($\sim 10^6 M_{\odot}$) “dark star” spectra. Detailed predictions of such emission in the context of the Pop III.1 cosmological model are still needed. However, if $d_{\text{iso}} \gtrsim 50$ kpc, then we expect most such stars only at $z \gtrsim 20$.

4.5. Occupation Fraction of SMBHs

BTM19 and SMT23 analyzed the SMBH occupation fractions, f_{SMBH} , of dark matter halos, i.e., what fraction of halos host SMBHs as a function of halo mass. For the case of $d_{\text{iso}} = 50$ kpc, by redshift of zero, f_{SMBH} reached unity for halos with masses $\gtrsim 10^{12} M_{\odot}$, while a level of $\sim 10\%$ seeding was present down to halo masses

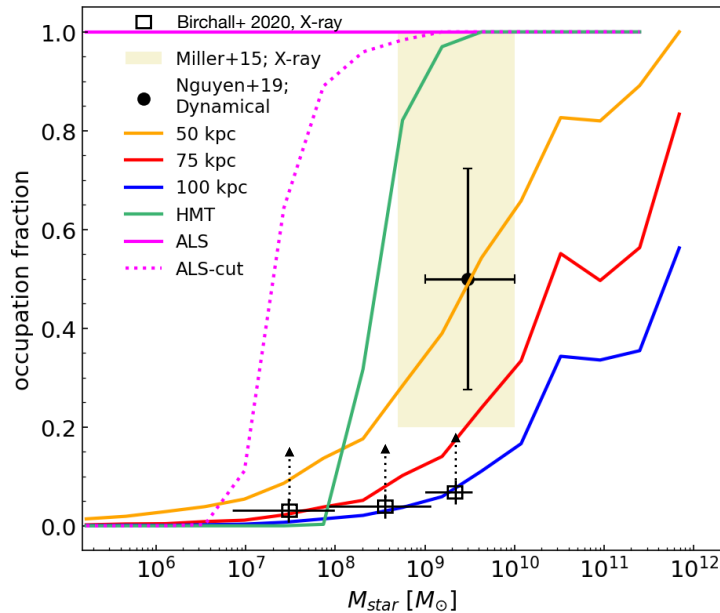


Fig. 7. (Adapted from CMT24) Occupation fraction of seeded galaxies as a function of stellar mass at redshift zero. The yellow, red and blue lines show Pop III.1 models with $d_{\text{iso}} = 50, 75, 100$ kpc. The green line shows an HMT model with threshold halo mass of $7.1 \times 10^{10} M_{\odot}$ for SMBH seeding. The solid pink line is an All Light Seeds (ALS) model, which seeds all halos with low-mass black holes, so has an occupation fraction of unity. The dotted pink line shows the ALS results only for SMBHs with masses $> 10^5 M_{\odot}$. The following observational constraints are shown: an X-ray survey result that yields a lower limit of about 0.2 in systems with $M_{\text{star}} \sim 10^9 - 10^{10} M_{\odot}$ (Miller et al. 2015); an X-ray survey of lower-mass systems that detects AGN (with $\log_{10} L_X / \text{erg s}^{-1} > 39$) in about 3-6% of the systems (Birchall et al. 2020); a study of the dynamical properties of the nuclei of a small sample of nearby galaxies (Nguyen et al. 2019).

of $\sim 10^{10} M_{\odot}$. As expected, occupation fractions become smaller as d_{iso} increases.

The CMT24 results for f_{SMBH} as a function of galaxy stellar mass are shown in Fig. 7. We see that a major difference between the different d_{iso} models and the HMT and ALS models is the occupation fraction for galaxies with $M_{\text{star}} \sim 10^9 M_{\odot}$. This figure also shows observational constraints, which, however, have large uncertainties. Nevertheless, these results indicate a preference for $d_{\text{iso}} \lesssim 75$ kpc.

4.6. Gravitational Wave Emission of SMBHs

Analysis of the North American Nanohertz Observatory for Gravitational Waves (NANOGrav) pulsar timing array (PTA) 15 yr data set has detected a signal consistent with that expected from a nHz gravitational wave background (GWB) with a false-alarm probability of $\sim 10^{-4} - 10^{-3}$ ($\simeq 3\sigma$) (Agazie et al. 2023a). The most natural explanation for this signal is the result of the cosmic population of SMBH

binaries (e.g., Agazie et al. 2023b). The planned Laser Interferometer Space Antenna (LISA) will operate at mHz frequencies and be sensitive to mergers of SMBH binaries with masses $\sim 10^4 - 10^8 M_\odot$ out to $z \sim 10$ (Amaro-Seoane et al. 2023).

The Pop III.1 model can be used to make predictions for the gravitational wave emission that emerges from the cosmic population of SMBH binaries. As mentioned above, one feature of Pop III.1 seeding is that SMBHs are born relatively isolated from each other. Thus, as shown in Fig. 5, mergers of seeded halos that would produce SMBH binaries occur only at relatively low redshifts, i.e., $z \lesssim 2$. Naturally, mergers start earlier and are more frequent in the models with smaller d_{iso} . SMT23 find that by $z = 0$ (and in the limit of fast merging of SMBHs once two seeded halos merge) the raw number of mergers in a $\sim (60 \text{ cMpc})^3$ volume rises from 191 (out of a total population of 1,234, i.e., 15.5%) for $d_{\text{iso}} = 100 \text{ kpc}$ to 3,305 (out of a total population of 15,400, i.e., 21.5%) for $d_{\text{iso}} = 50 \text{ kpc}$.

To make predictions for the GWB from a given SMBH seeding model, two main astrophysical processes need to be modeled: 1) the growth of SMBHs; 2) the timescale for SMBH binary merging following halo merger. Each of these processes are complicated and it is difficult to make accurate predictions (see, e.g., Agazie et al. 2023b). For SMBH growth, as an alternative to modeling, one can resort to empirical scaling relations between host galaxy properties and SMBH mass.

Preliminary work examining the implications of the Pop III.1 model for the GWB has been presented by Singh (2024), but with more detailed calculations underway (Singh et al., in prep.). Preliminary findings are that the nHz GWB can be reproduced if reasonable, empirical assumptions about SMBH growth are made, however, the results are sensitive to treatment of the most massive SMBHs and their merger rates. Given the relatively large contribution from the most massive systems, the amplitude of the GWB is relatively insensitive to d_{iso} , i.e., with only a factor of ~ 3 increase as d_{iso} decreases from 100 kpc to 50 kpc. We anticipate that greater sensitivity to d_{iso} will be present in higher order statistics of the GWB, e.g., the relative contribution of strongest individual sources, which also impart large scale asymmetries in the GWB (e.g., Gardiner et al. 2024).

In terms of predictions for the rate of SMBH merger events that will be detectable by LISA, scaling to the volume of the Universe out to $z = 2$, i.e., $\sim 600 \text{ cGpc}^3$, from the results of SMT23 for $d_{\text{iso}} = 100 \text{ kpc}$ we expect 5.3×10^8 mergers to occur. In the limit of fast merging time of SMBHs after halo merger and if these occur at a uniform rate over the lookback time of $\sim 10 \text{ Gyr}$, then this implies an event rate of 0.05 yr^{-1} . The equivalent rate for $d_{\text{iso}} = 50 \text{ kpc}$ is 0.9 yr^{-1} . Most of these mergers are expected to be detectable by LISA, especially given a fiducial Pop III.1 seed mass of $\sim 10^5 M_\odot$. Thus we see that the overall event rate that LISA may detect, e.g., in a nominal 4-year mission lifetime, is very sensitive to the isolation distance parameter. Another key prediction of the Pop III.1 models is the redshift distribution of the events. For the $d_{\text{iso}} = 50 \text{ kpc}$ case this extends to moderately higher redshifts ($z \simeq 2.5$) compared to the $d_{\text{iso}} = 100 \text{ kpc}$ case ($z \simeq 1.5$). However,

the main prediction is that all events should be at these relatively low redshifts.

4.7. Contribution to Cosmic Reionization

A key prediction of the Pop III.1 model is the existence of large (~ 1 cMpc) HII regions around supermassive Pop III.1 stars at $z \sim 20 - 30$. These HII regions fill a large fraction of the volume of the Universe at these redshifts, but recombine on timescales of $\sim 50 - 200$ Myr, i.e., down to $z \sim 15$. Such sources could make a significant contribution to the Thomson scattering optical depth of CMB photons. From preliminary modeling using the BEoRN code (Schaeffer et al. 2023) of such HII regions around Pop III.1 stars (la Torre et al., in prep.), this contribution to the total $\tau_{\text{CMB}} \simeq 0.055$ rises from $\sim 6\%$ for $d_{\text{iso}} = 100$ kpc to $\sim 36\%$ for $d_{\text{iso}} = 50$ kpc.

The E -mode CMB polarization power spectrum has some sensitivity to the redshift dependence of reionization history (e.g., Heinrich et al. 2017; Millea & Bouchet 2018). Future CMB polarization observations, e.g., with LiteBIRD (Allys et al. 2023) will be able to improve on such constraints. In addition, future CMB observations with the Simons Observatory (Ade et al. 2019) will be able to test the Pop III.1 prediction of the presence of an early phase of partial cosmic reionization, in particular via observation of the “patchy” kinematic Sunyaev-Zel’dovich (kSZ) effect from the peculiar motion of free electron bubbles around these first stars.

The ionized bubbles around Pop III.1 sources may also be detectable in surveys of high- z 21 cm emission. For example, the Hydrogen Epoch of Reionization Array (HERA; Abdurashidova et al. 2022) has sensitivity to such emission out to $z \sim 28$ and may be able to detect if there is a characteristic size of such bubbles.

5. Implications for Dark Matter

The Pop III.1 mechanism for SMBH formation *requires* energy injection from decaying dark matter. This dark matter particle has so far been assumed to be a WIMP (e.g., Spolyar et al. 2008; Natarajan et al. 2009; Rindler-Daller et al. 2015). While there is some dependence of the protostellar initial condition and early evolution to the WIMP mass (Natarajan et al. 2009; see Fig. 2), we anticipate that the primary sensitivity of the model to particle properties is via the spin-dependent scattering cross section, i.e., of WIMPs with protons. This is because for growth to supermassive scales in a large, swollen state the protostar needs to continue capture WIMPs from the surrounding minihalo. However, to make accurate calculations of this rate and its sensitivity to assumed particle properties (e.g., Aalbers et al. 2024), requires accurate knowledge of the surrounding dark matter density. This requires modeling adiabatic contraction of the dark matter in the minihalo caused by the slow baryonic contraction of the Pop III.1 protostellar infall envelope. Finally, given the current non-detection of WIMPs, we note that more exotic forms of cold dark matter, even including very low-mass primordial black holes (e.g., Carr & Kuhnel 2020), could allow the Pop III.1 mechanism to operate, with the main requirement that the dark matter inject energy inside these early protostars.

6. Summary

The Pop III.1 cosmological model for SMBH formation (BTM19, SMT23, CMT24) invokes dark matter annihilation heating in first-forming, undisturbed minihalos, where slow baryonic collapse leads to adiabatic contraction of the dark matter density. Only under such specialized conditions does the dark matter particle number density reach high enough levels for there to be significant annihilation heating that impacts protostellar structure (Spolyar et al. 2008; Natarjan et al. 2009; Rindler-Daller et al. 2015) to maintain large, cool photospheres that have limited ionizing feedback allowing growth of supermassive Pop III stars and thence SMBHs.

The Pop III.1 model naturally produces a characteristic mass of SMBH seeds of $\sim 10^5 M_\odot$, with this related to the baryonic content of $\sim 10^6 M_\odot$ dark matter minihalos. In contrast to other formation theories, the Pop III.1 model explains why there is a paucity of IMBHs. A phase of ionizing feedback from supermassive Pop III.1 protostars that emit $\sim 10^{53}$ H-ionizing photons per second sets the overall cosmic abundance of SMBHs, which is expected to be $\lesssim 0.2 \text{ cMpc}^{-3}$. Most minihalos, having been exposed to ionizing radiation that elevates their free electron abundance, fragment into $\sim 10 M_\odot$ Pop III.2 stars that do not adiabatically contract their dark matter. The SMBH seed population is formed very early: they are all in place by $z \sim 20$. After this the SMBH co-moving number density is nearly constant until mergers begin to occur by $z \lesssim 2$. Additional predictions are: a low level of initial clustering of SMBHs; a low level of binary SMBHs (and associated mergers) at high z ; and ionized, $\sim 1 \text{ cMpc}$ -sized bubbles at $z \gtrsim 20$ that contribute to partial early cosmic reionization.

To the extent that the Pop III.1 model is needed to explain the existence of all (or the majority) of SMBHs, there are implied constraints on the nature of dark matter. In particular, for self-annihilating WIMPs, these particles must be captured at sufficient rates into Pop III.1 protostars to allow protostellar growth to $\sim 10^5 M_\odot$.

Acknowledgments

We thank the following collaborators, especially in the SMBH and HUDF groups, for their help in developing and testing the Pop III.1 seeding model: G. Abramo; N. Banik; E. Blackman; K. Chanchaiworawit; O. Cray; R. Ellis; F. Fontanot; K. Fridell; I. Georgiev; Y. Harikane; M. Hayes; B. Keller; M. la Torre; N. Laporte; C. McKee; A. Natarajan; R. O'Reilly; B. O'Shea; A. Saxena; K. Tanaka; K. Topalakis; A. Young. We also thank the following colleagues for helpful discussions: B. Draine; X. Fan; K. Freese; C. Hill; C. Ilie; A. Lidz; G. Meynet; D. Spergel; N. Yoshida. JCT acknowledges support from ERC Advanced Grant 788829 (MSTAR) and the CCA Sabbatical Visiting Researcher program.

References

1. Aalbers, J. et al. 2024, Physical Review D, Vol. 109, Issue 9, article id.092003
2. Abdurashidova, Z. et al. 2022, ApJ, 925, 221
3. Abel T., Bryan G. L., & Norman M. L., 2002, Science, 295, 93
4. Ade, P. et al. 2019, JCAP, Issue 02, article id. 056
5. Agazie, G. et al. 2023, ApJ Lett., 951, L8
6. Agazie, G. et al. 2023, ApJ Lett., 952, L37
7. Allys, E. et al. 2023, PTEP, Vol. 2023, Issue 4, id.042F01
8. Amaro-Seoane, P., et al. 2023, LRR, 26, 2
9. Baldassare V. F., Reines A. E., Gallo E. & Greene J. E. 2015, ApJ, 809, L14
10. Banik N., Tan J. C., Monaco P., 2019, MNRAS, 483, 3592
11. Baumgardt, H. 2017, MNRAS, 464, 2174
12. Baumgarte T. W. & Shapiro S. L. 1999, ApJ, 526, 941
13. Birchall, K. L., Watson, M. G., & Aird, J. 2020, MNRAS, 492, 2268
14. Bogdán, A., Goulding, A., Natarajan, P. et al. 2024, Nature Astronomy, Vol. 8, 126
15. Bouwens, R. J., Illingworth, G. D., Oesch, P. A. et al. 2010, ApJL, 709, L133
16. Bromm V., Coppi P. S. & Larson R. B., 2002, ApJ, 564, 23
17. Bromm V. & Loeb A., 2003, ApJ, 596, 34
18. Buchert T. & Ehlers J. 1993, MNRAS, 264, 375
19. Cammelli, V., Monaco, P., Tan, J. C. et al. 2024, MNRAS, in press (arXiv:2407.09949) [CMT24]
20. Carr, B. & Kuhnel, F. 2020, Ann. Rev. Nucl. Part. Sci., 70, 355
21. Catelan P. 1995, MNRAS, 276, 115
22. Chandrasekhar S. 1964, ApJ, 140, 417
23. Chon S., Hirano S., Hosokawa T. & Yoshida N., 2016, ApJ, 832, 134
24. Ellis, R. S., McLure, R. J., Dunlop, J. S., et al. 2013, ApJL, 763, L7
25. Fontanot, F., De Lucia, G., Hirschmann, M. et al. 2020, MNRAS, 496, 3943
26. Freese K., Ilie C., Spolyar D., Valluri M., & Bodenheimer P. 2010, ApJ, 716, 1397
27. Freitag, M., Gürkan, M. A. & Rasio, F. A. 2006, MNRAS, 368, 141
28. Gardiner, E. C., Kelley, L. Z., Lemke, A.-M. & Mitridate, A. 2024, ApJ, 965, 164
29. Greene, J. E., Strader, J., Ho, L. S. 2020, ARA&A, 58, 257
30. Greif T. H. & Bromm V., 2006 MNRAS, 373, 128
31. Gürkan, M. A., Freitag, M., & Rasio, F. A. 2004, ApJ, 604, 632
32. Häberle, M., Neumayer, N., Seth, A. et al. 2024, Nature, Vol. 631, Issue 8020, 285
33. Haehnelt M. G. & Rees M. J. 1993, MNRAS, 263, 168
34. Harikane, Y., Zhang, Y., Nakajima, K. et al. 2023, ApJ, 959, 39
35. Hayes, M., Tan, J. C., Ellis, R. et al. 2024, ApJL, 971, L16
36. Heger, A. & Woosley, S. E. 2002, ApJ, 567, 532
37. Heinrich, C. H., Miranda, V. & Hu, W. 2017, PRD, Vol. 95, Issue 2, id.023513
38. Hennawi, J. F., Strauss, M. A., Oguri, M. et al. 2006, AJ, 131, 1
39. Hickox, R. C., Jones, C., Forman, W. R. et al. 2009, ApJ, 696, 891
40. Hirano, S., Hosokawa, T., Yoshida, N. et al. 2014, ApJ, 781, 60
41. Hosokawa T., Omukai K., Yoshida N. & Yorke H. W., 2011, Science, 334, 1250
42. Ilie, C., Paulin, J., & Freese, K. 2023, PNAS, Vol. 120, Issue 30, article id.e2305762120
43. Johnson, J. L. & Bromm, V. 2006, MNRAS, 366, 247
44. Jungman, G., Kamionkowski, M. & Griest, K. 1996, Phys. Rep., 267, 195
45. Kormendy J. & Ho L. C. 2013, ARA&A, 51, 511
46. Kocevski D. D., et al. 2023, ApJ, 954, L4
47. Latif M. A. & Schleicher D. R. G., 2016, A&A, 585, 151
48. Latif, M. A., Whalen, D. et al. 2022, Nature, Vol. 607, 7917, 48

49. Li J., Silverman, J. D., Shen, Y. et al. 2024, ApJ, sub. (arXiv:2403.00074)
50. Liepold, E. R. & Ma, C. 2024, ApJ Lett., 971, L29
51. Lyu, J., Alberts, S., Rieke, G. H. & Rujopakarn, W. 2022, ApJ, 941, 191
52. Maiolino, R., Scholtz, J., Witstok, J. et al. 2024, Nature, Vol. 627, 8002, 59
53. Maiolino, R., Scholtz, J., Curtis-Lake, E. et al. 2024, A&A, 691, 145
54. Matsuoka, Y., Izumi, Takuma, T., Onoue, M. et al. 2024, ApJ, 965, L4
55. McKee C. F. & Tan J. C., 2008, ApJ, 681, 771
56. Millea, M. & Bouchet, F. 2018, A&A, 617, A96
57. Miller B. P., Gallo E., Greene J. E. et al. 2015, ApJ, 799, 98
58. Monaco P., Sefusatti E., Borgani S. et al. 2013, MNRAS, 433, 2389
59. Monaco P., Theuns T. & Taffoni G. 2002, MNRAS, 331, 587
60. Moutarde F., Alimi J.-M., Bouchet F. R., Pellat R., Ramani A., 1991, ApJ, 382, 377
61. Mummery, A. & van Velzen, S. 2024, MNRAS, sub. (arXiv:2410.17087)
62. Mutlu-Pakdil, B., Seigar, M. S. & Davis, B. L. 2016, ApJ, 830, 117
63. Nakajima, K., Ouchi, M., Isobe, Y. et al. 2023, ApJS, 269, 33
64. Natarajan A., Tan J. C. & O'Shea B. W. 2009, ApJ, 692, 574
65. Nguyen D. D., et al., 2019, ApJ, 872, 104
66. Pacucci, F., Nguyen, B., Carniani, S., Maiolino, R., Fan X. 2023, ApJ, 957, L3
67. Paxton, B., Cantiello, M., Arras, P. et al. 2013, ApJS, 208, 4
68. Rees M. J., 1978, The Observatory, 98, 210
69. Reines A. E. & Volonteri M. 2015, ApJ, 813, 82
70. Reines A. E. & Comastri A., 2016, PASA, 33, 54
71. Rindler-Daller T., Montgomery M. H., Freese K. et al. 2015, ApJ, 799, 210
72. Rosdahl, J., Blaizot, J., Aubert, D. et al. 2013, MNRAS, 436, 2188
73. Schaeffer, T., Giri, S. K., Schneider, A. 2023, MNRAS, 526, 2942
74. Schleicher, D. R. G., Reinoso, B., Latif, M. et al. 2022, MNRAS, 512, 6192
75. Shankar, F. et al. 2020, Nature Astronomy, 4, 282
76. Singh, J. 2024, Ph.D. thesis, University of Trieste
77. Singh, J., Monaco, P., Tan, J. C. 2023, MNRAS, 525, 969 [SMT23]
78. Smith R. J., Iocco F., Glover S. et al. 2012, ApJ, 761, 154
79. Spolyar D., Freese K. & Gondolo P. 2008, Phys. Rev. Lett., 100, 051101
80. Stacy A., Pawlik A. H., Bromm V. & Loeb A., 2014, MNRAS, 441, 822
81. Susa H., Hasegawa K. & Tominaga N., 2014, ApJ, 792, 32
82. Tan, J. C., Beltran, M. T., Caselli, P. et al. 2014, Protostars & Planets VI, p149
83. Tan J. C. & Blackman E. G., 2004, ApJ, 603, 401
84. Tan J. C. & McKee C. F., 2004, ApJ, 603, 383
85. Tan, J. C., Smith, B. D., & O'Shea, B. W. 2010, AIP Conf. Proc., Vol. 1294, 34
86. Tanaka, K. E. I., Tan, J. C. & Zhang, Y. 2017, ApJ, 835, 32
87. Übler H., Maiolino, R., Curtis-Lake, E. et al., 2023, A&A, 677, A145
88. Vika M., Driver S. P., Graham A. W., Liske J., 2009, MNRAS, 400, 1451
89. Vogelsberger M., et al. 2014, Nature, 509, 177
90. Volonteri, M., Habouzit, M. & Colpi, M. 2021, Nature Reviews Physics, 3, 732
91. Wang, F., Jinyi, Y., Fan, X. et al. 2021, ApJ Letters, 907, L1
92. Weinberger, R., Springel, V., Hernquist, L. et al. 2017, MNRAS, 465, 3291
93. Wise, J. H., Regan, J. A., O'Shea, B. W. et al. 2019, Nature, 566, 7742
94. Wu, Q. & Shen, Y. 2022, ApJS, 263, 42
95. Yang, J., Wang, F., Fan, X. et al. 2021, ApJ, 923, 262
96. Yue, M., Fan, X., Yang, J. & Wang, F. 2021, ApJ Lett., 921, L27
97. Yue, M., Fan, X., Yang, J. & Wang, F. 2023, AJ, 165, 191
98. Zeltyn, G., Trakhtenbrot, B., Eracleous, M. et al. 2024, ApJ, 966, 85